Non-degenerate parametric mixing and Qenhancement in ALN Lamb wave resonator

Cite as: Appl. Phys. Lett. **118**, 254101 (2021); https://doi.org/10.1063/5.0053818 Submitted: 12 April 2021 • Accepted: 05 June 2021 • Published Online: 21 June 2021

🗓 Ting Lu, 🗓 Joseph D. Schneider, 🗓 Sidhant Tiwari, et al.







ARTICLES YOU MAY BE INTERESTED IN

Al_{0.68}Sc_{0.32}N Lamb wave resonators with electromechanical coupling coefficients near 10.28%

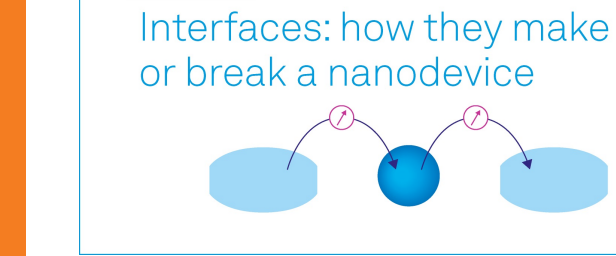
Applied Physics Letters 118, 171902 (2021); https://doi.org/10.1063/5.0047647

Transducer design for AIN Lamb wave resonators

Journal of Applied Physics 121, 154502 (2017); https://doi.org/10.1063/1.4979914

Frequency conversion through nonlinear mixing in acoustic waves

Journal of Applied Physics 128, 064105 (2020); https://doi.org/10.1063/5.0018074



Webinar



March 29th - Register now





Non-degenerate parametric mixing and Q-enhancement in ALN Lamb wave resonator

Cite as: Appl. Phys. Lett. 118, 254101 (2021); doi: 10.1063/5.0053818

Submitted: 12 April 2021 · Accepted: 5 June 2021 ·

Published Online: 21 June 2021







Ting Lu, ¹ D Joseph D. Schneider, ^{2,3} D Sidhant Tiwari, ¹ Xiating Zou, ¹ Lap K. Yeung, ¹ Robert N. Candler, ^{1,4} D Gregory P. Carman, ² D and Yuanxun Ethan Wang ^{1,a)} D

AFFILIATIONS

- ¹Electrical and Computer Engineering Department, UCLA, Los Angeles, California 90095, USA
- ²Mechanical and Aerospace Engineering Department, UCLA, Los Angeles, California 90095, USA
- ³Lawrence Livermore National Laboratory, Livermore, California 94550, USA
- ⁴California Nano Systems Institute, Los Angeles, California 90095, USA

ABSTRACT

In this Letter, we explore a non-degenerate phase independent parametric quality factor (Q)-enhancement technique for aluminum nitride (AlN) Lamb wave resonators. Unlike other active Q-enhancement techniques which require precise phase control of the electronic feedback loop, this technique is implemented by parametrically pumping AlN material stiffness to realize a negative resistance seen at the signal path. The negative resistance is dependent on the nonlinear material modulation and multi-resonance coupling in the device. A nonlinear circuit model is developed to simulate the parametric coupling of each resonance and extract the nonlinearity of AlN from experimental data. With proper pump frequency and pump power, the device quality factor is boosted in both simulation and experiment. The demonstrated Q-enhancement method is simple to implement and can be applied to other types of resonators that have nonlinear behavior and support multi-resonance operation.

Published under an exclusive license by AIP Publishing. https://doi.org/10.1063/5.0053818

Acoustic wave resonators have been widely used for filters and diplexers in radio frequency mobile device front-ends due to their excellent performance (i.e., low insertion loss and high quality factor) and small footprint compared to their electronic counterparts. Among various acoustic wave devices, the Lamb wave resonator recently gained attention because it has both fundamental strengths of commercial surface acoustic wave (SAW) resonators and bulk acoustic wave (BAW) resonators: lithographically defined resonance frequency and CMOS circuit compatibility. The fundamental symmetric Lamb wave mode propagating in aluminum nitride (AlN) thin films exhibits a very high phase velocity of up to 10 000 m/s and thus supports higher frequency operation than the surface acoustic wave. However, for the center frequency considered in this work (>300 MHz), the Lamb wave resonator suffers from damping and Q degradation, mainly caused by the large anchor loss. 11,12

It has been demonstrated that Q-enhancement methods can be applied to an acoustic resonator to boost the device's Q.¹³ Passive Q-enhancement technique can be attained lithographically without adding to the power requirement to the system; however, it relies on the specific device geometry to confine energy.^{14,15} Active-feedback

Q-enhancement technique with external electronics can break the intrinsic fundamental limit of the material quality factor, but it requires precise gain and phase control 16,17 and may introduce additional noise. Parametric pumping is a technique for feeding energy into a dynamical system by modulating the reactive parameter of the system. 18 Degenerate parametric Q-enhancement has been studied extensively in low-frequency micromechanical resonator systems. It is achieved by modulating the spring constant at exactly twice the resonant frequency, and it requires a precise in-phase condition between the pump and intrinsic resonance. 19-22 Non-degenerate parametric enhancement, on the other hand, is phase and frequency independent. However, significant efforts investigating acoustic parametric Q-enhancement for radio frequency above 300 MHz have not been reported, as nonlinear compliance in most piezoelectric material is negligible for practical applications. Recently, researchers have reported observing nonlinear compliance and frequency conversion^{23,24} in AlN Lamb wave devices. This suggests that AlN has the potential to demonstrate parametric Q-enhancement effects.

In this Letter, a non-degenerate phase independent parametric pumping technique is proposed to improve the Q of an AlN Lamb

a) Author to whom correspondence should be addressed: ywang@ee.ucla.edu

wave resonator. The proposed technique utilizes a negative resistance, which originates from the parametric amplification effect ^{25,26} and has been recently applied in microwave LC resonators. ^{27,28} For Q-enhancement, the AlN's mechanical stiffness is modulated, thus realizing a negative resistance seen at the signal path. In order to reduce the damping of the acoustic resonator, a Lamb wave resonator supporting harmonics operation has been designed, fabricated, and tested. A multi-resonance coupled nonlinear model is developed to simulate the parametric coupling of each resonance and extract the nonlinearity of AlN. Parametric mixing and Q-enhancement have been demonstrated in both the simulation and the experiment. This multi-resonance coupled nonlinear model and Q-enhancement technique can be applied to other types of resonators that have the nonlinear behavior and support multi-resonance operation.

Figure 1 shows the concept of negative-resistance parametric Q-enhancement. For simplicity, the three-wave mixing circuit model shown in Fig. 1(a) is considered. Assume that only power at pump frequency f_p , signal frequency f_s , and idler frequency f_{p-s} can go in/out of

the varactor (i.e., capacitor with a voltage tunable capacitance). The Manley–Rowe relation²⁹ predicts that pump power supplied to the nonlinear capacitance will deliver positive power to the signal path and, thus, realize signal power gain. Specifically, when the nonlinear capacitance is modulated by the large pump power, as shown in Fig. 1(b), the capacitance variation can be written in the form of

$$C(t) = C_0 + 2\xi C_0 \cos(\omega_p t), \tag{1}$$

where ξ is the nonlinear modulation of the capacitance and C_0 is the static capacitance. The equivalent admittance of the nonlinear capacitor at signal frequency f_s is given as

$$Y_{var} = j\omega_s C_0 - \frac{\omega_s \omega_{p-s} \xi^2 C_0^2}{Y_{p-s}^* - j\omega_{p-s} C_0},$$
 (2)

where Y_{p-s} is the admittance of the idler path [the series combination L_{p-s} , C_{p-s} and R_{p-s} in Fig. 1(b)]. The second term in Eq. (2) is equivalent to a negative conductance G in Fig. 1(c) when Y_{p-s}^* is made to

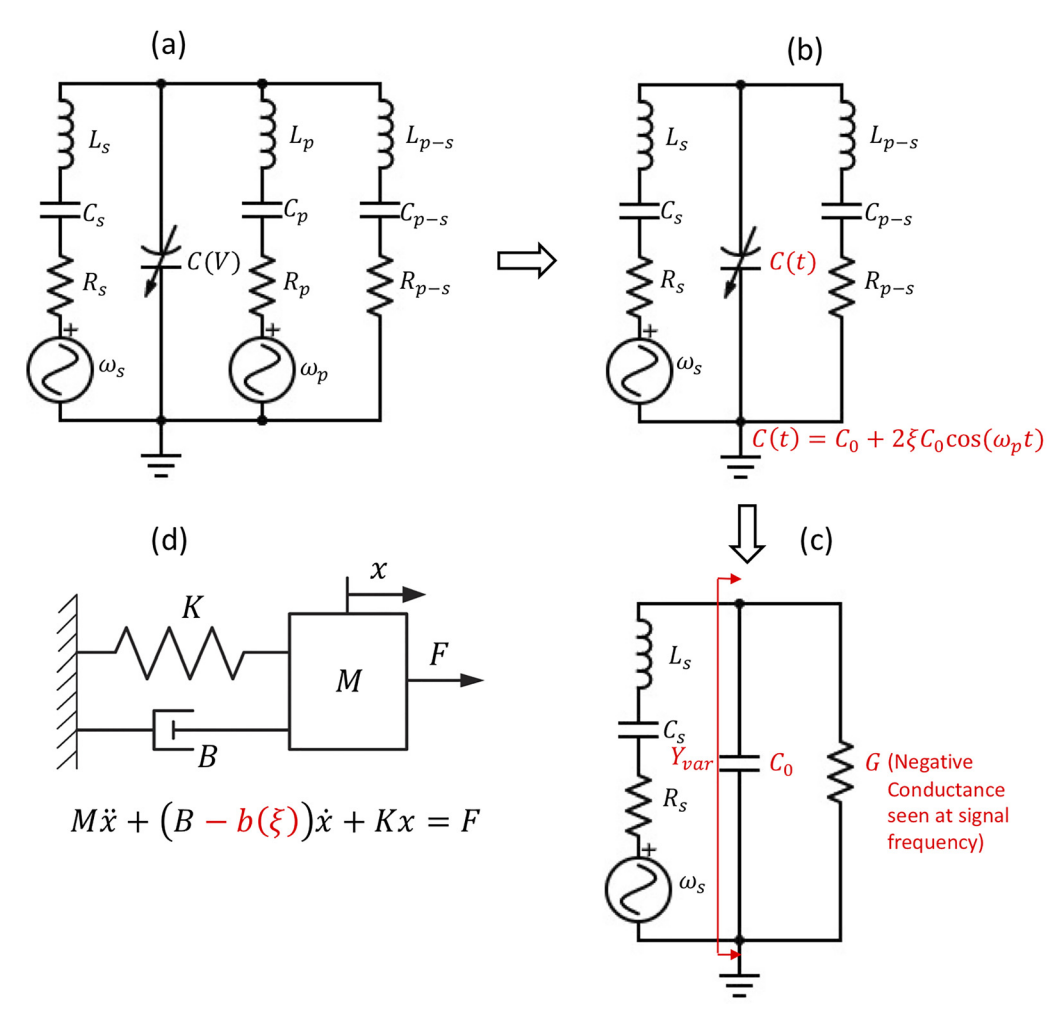


FIG. 1. Negative-resistance parametric Q-enhancement concept. (a) Three-wave mixing circuit model, (b) time-varying and parametric pumped nonlinear capacitor, (c) the negative conductance seen at the signal frequency, (d) the analogy of the signal path to a mechanical system with the reduced damping. M is the mass of the system, B is the damping, and K is stiffness.

resonate with C_0 at f_{p-s} , or equivalently, $Y_{p-s}^* - j\omega_{p-s}C_0 = G_{p-s}$, where G_{p-s} accounts for the resonator loss at f_{p-s} due to the finite quality factor Q_{p-s} . Thus, as shown in Fig. 1(c), the signal path sees a negative conductance G in parallel with a normal capacitor C_0 , which reduces the loss of the signal resonator and enhances the quality factor. The negative conductance G can be further normalized by the signal conductance G_s and becomes

$$\frac{G}{G_s} = -\xi^2 Q_s Q_{p-s},\tag{3}$$

where Q_s and Q_{p-s} represent the quality factor of the signal resonance and the idler resonance, respectively. More details about mathematical derivations can be found in the supplementary material. The negative-resistance Q-enhancement concept is equivalent to the Q-enhancement in the mechanical system shown in Fig. 1(d), where the damping is reduced by the negative-resistance technique. In summary, this technique is subject to the following conditions: (1) the nonlinear capacitor is shared by signal, pump, and idler path and is modulated by large pump power, and (2) the idler path is in resonance with the static capacitance at the idler frequency f_{p-s} .

Acoustic waves are analogous to electromagnetic waves.³⁰ The capacitance in electromagnetic waves is analogous to the mechanical compliance in acoustic waves. An AlN thin film is chosen for this

study because nonlinear mechanical stiffness in AlN thin film is analogous to a varactor in the resonator model and can be exploited to demonstrate the parametric Q-enhancement behavior shown in Fig. 1. Figure 2 shows the two-port Lamb wave resonator designed for demonstrating the parametric effects. The 400 nm AlN film is used because the thickness is much shorter than operating wavelength of the resonator (18.4 μ m); therefore, the first order symmetric mode (S_0) is the primary operating mode in the resonator⁸ and it has a higher phase velocity compared to that in the thicker AlN film. Higher harmonics like the second and third orders of the S_0 mode (frequency equal to, or close to if dispersive, twice and triple of the fundamental mode resonance) are also supported in the resonator. The parametric Qenhancement concept relies on coupling the signal resonance (fundamental mode resonance) and the idler resonance (second-order mode resonance). When the pump power P_p induces a time varying nonlinear mechanical compliance in AlN, signal power P_s and idler power P_{p-s} are coupled by the parametrically pumped compliance. Because the idler is at resonance, the signal path sees a negative conductance, which boost the quality factor of the signal resonance. To launch signal power and pump power, two sets of interdigitated transducers (IDTs) (34 fingers each) with the grounded bottom electrode convert electrical energy into acoustic energy and, conversely, acoustic energy into electrical energy through the piezoelectric effect. As shown in Fig. 2(a), the

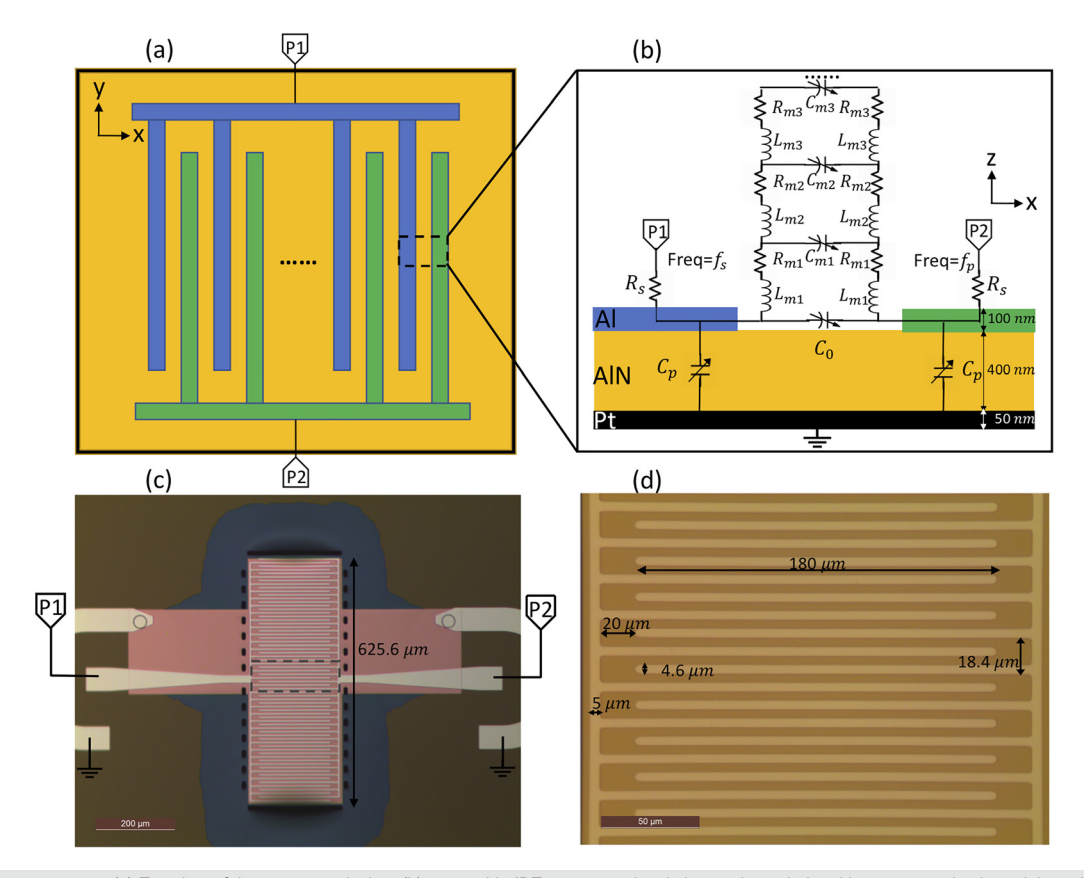


FIG. 2. Lamb wave resonator. (a) Top view of the resonator design, (b) zoomed in IDTs cross-sectional view and coupled multi-resonance circuit model overlaying the device. (c) Optical image of the Lamb wave devices after fabrication. The blue area under the IDTs is where the Si has been etched. (d) Zoomed in dashed region of (c) with IDT dimensions.

upper set of IDTs (in blue) is responsible for exciting the signal resonance at f_s , and the lower set of IDTs (in green) feeds the pump power at f_p .

Figure 2(b) shows the zoomed in IDT cross section and the schematic of the coupled multi-resonance model. Each circuit element is the parallel combination of all subelements that appear between the top metal fingers and the bottom electrode. The coupled multiresonance model is built based on the transmission line theory. Acoustic wave propagation in a piezoelectric material is analogous to EM wave propagation in a transmission line waveguide, which can be modeled as cascaded sections of series inductors (L_{m1} , L_{m2} , L_{m3} ...) and parallel capacitors (C_{m1} , C_{m2} , C_{m3} ...). Acoustic wave resonators have edge reflectors that can be modeled as open boundaries to the transmission line model. Series resistors (R_{m1} , R_{m2} , R_{m3} ...) are added to the model to represent the loss of resonance. When only one resonance is of interest, this multi-resonance model can be degenerated to the mBVD (modified Butterworth-Van Dyke) model^{1,31} by keeping only one section of the resistor (R_{m1}) , inductor (L_{m1}) , and capacitor (C_{m1}) . The capacitance between the IDT fingers (C_0) and static resistance (R_s) and the capacitance between top IDT and bottom grounded electrode (C_p) are included in the model. For nonlinear simulation, capacitors are replaced by varactors to represent the nonlinearity of AlN. Circuit parameters of the coupled multi-resonance model can be found in the supplementary material.

Figure 2(c) shows an optical image of the fabricated Lamb wave resonator. The fabrication process can be found in the Appendix of Ref. 32. The blue area under the IDTs is where the Si has been etched. Slotted release vents are applied to support a wider resonator, which allow for more IDT fingers to lower the motional resistance R_m . Lowered R_m makes the resonator easy to be integrated with the existing 50 Ω systems. However, slotted release vents increase the number of anchors in the resonator to 30. Multiple anchors result in insufficient confinement in the anchor direction and greatly increase the anchor loss and spurious modes. Figure 2(d) shows the zoomed in dashed region of Fig. 2(c), with the IDT dimensions labeled. The IDT width (4.6 μ m) is designed based on the signal resonance frequency (467 MHz) and the wave speed of the device (approximately 8574 m/s). Each set of the IDTs is connected to three pads designed for ground–signal–ground (GSG) probes with the 150 μ m pitch.

The Lamb wave resonator was first tested linearly by connecting P1 and P2 of the device to the ports of the vector network analyzer (VNA). S-parameters were measured to obtain the precise frequency of the first resonance and second resonance. The linear measurement is essential for determining the pump frequency in the Qenhancement measurement, in order to satisfy the frequency relation and idler resonance requirement. Figure 3 shows the experimental (solid blue line) and circuit simulated (dashed red line) magnitude of the (a) reflection coefficient and (b) insertion loss in the Lamb wave resonator for the first, second, and third resonances (i.e., first, second, and third harmonics of the So mode) with Q of each resonance extracted and labeled. Other modes that appear in the frequency bands are spurious modes mainly from acoustic waves interacting with the anchoring,³³ i.e., insufficient confinement in the anchor direction due to multiple anchors. The multi-resonance coupled circuit model agrees well with the experimental result, especially for the range of the resonance frequency. The first resonance has a minimum insertion loss of 10 dB at 467 MHz and serves as the signal resonance f_s . The

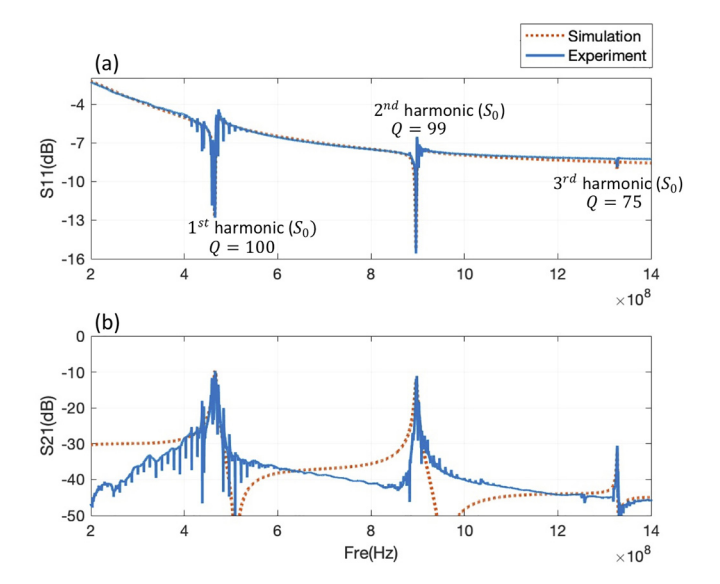


FIG. 3. Magnitude of S parameter: (a) reflection coefficient and (b) insertion loss for the Lamb wave resonator linear measurement. The blue solid line is the measurement result, and the red dashed line is from the circuit model.

electromechanical coupling factor k_t^2 is 1.71%. The second resonance has a minimum insertion loss of 11 dB at 897 MHz and serves as the idler resonance f_{p-s} . Ideally, if the second resonance f_{p-s} lies exactly at twice of the first resonance f_s , pump frequency f_p will lie at the third resonance. This is optimal because the insertion loss is the lowest at resonance (i.e., more pump power can go into the device). However, because of dispersion (i.e., lowered phase velocity of S_0 mode as frequency increases⁸), the pump frequency ($f_p = f_s + f_{p-s} = 1364 \, \text{MHz}$) is off from the third resonance (1327 MHz) and has an insertion loss of 45 dB. The insertion loss sets the requirement for high pump power in the Q-enhancement measurement.

The parametric frequency mixing experiment was then conducted to demonstrate the nonlinearity of the device and extract the nonlinear coefficient for the circuit model. The experimental setup is included in the supplementary material. Figure 4 shows experimental (right) and simulation (left) data of the parametric frequency mixing phenomenon in the Lamb wave resonator. The frequency mixing is caused by nonlinear compliance in AlN, i.e., frequency mixing would not occur in a linear material. The data presented in Figs. 4(a) and 4(b) show the mixing power P_{p-s} vs two different pump power levels $P_p = -6$, 4 dBm when the signal power P_s is fixed at 6 dBm, while Figs. 4(c) and 4(d) show the mixing power P_{p-s} vs two different signal power levels $P_s = -4$, 6 when pump power P_p is fixed at 4 dBm. In Fig. 4(b), mixing power P_{p-s} increases by approximately 10 dB when pump power P_p is increased by 10 dB. Similarly, mixing power P_{p-s} increases by approximately 10 when signal power P_s increases by 10 dB, as shown in Fig. 4(d). The linear dependency of mixing power P_{p-s} on input power is explained and discussed in Ref. 23. To briefly summarize, when material's compliance modulation (ξ) is small, ξ is linearly proportional to the amplitude of input voltage; thus, mixing power is also linearly proportional to the input power. The developed coupled multi-resonance circuit model shows similar trends to the experimental data for all the power conditions, as shown in

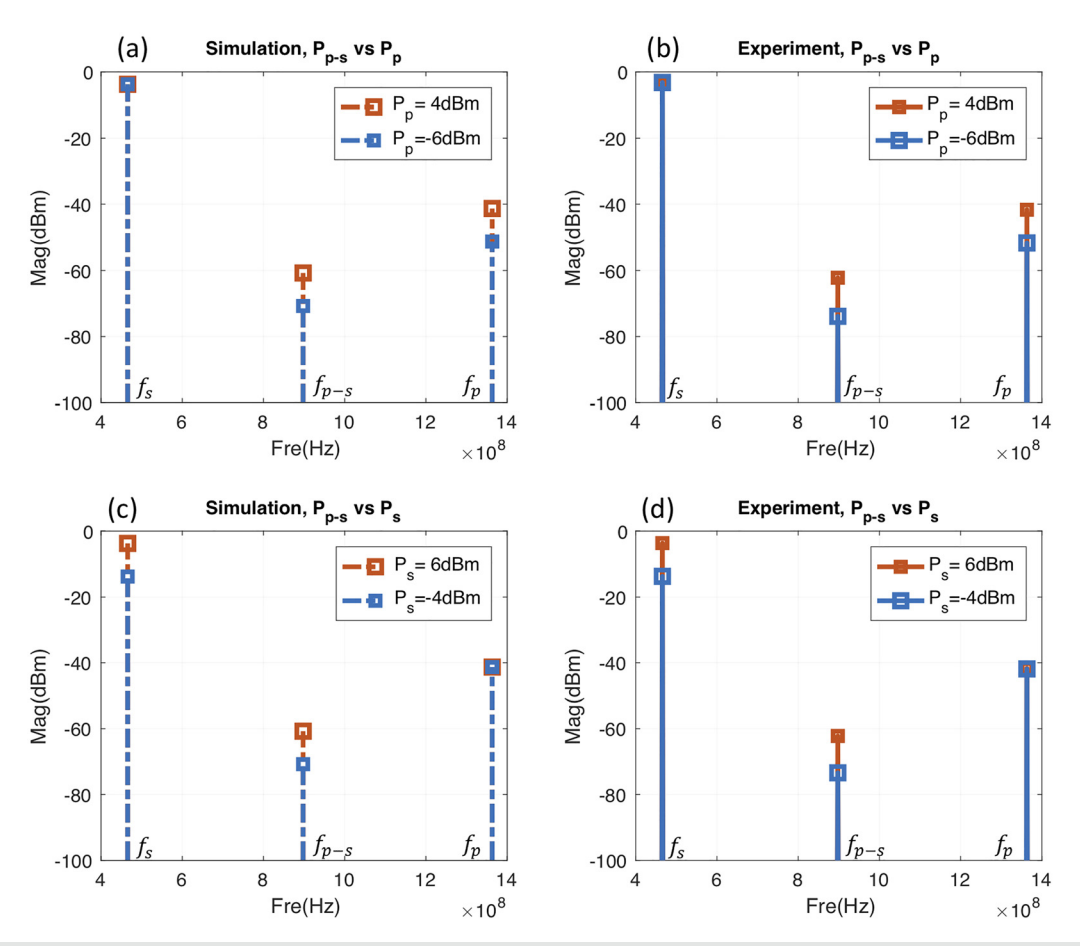


FIG. 4. Parametric frequency mixing results. (a) Simulation and (b) measurement results of mixing power P_{p-s} vs different pump power levels ($P_p = -6$ and $P_p = 4$ dBm), signal power P_s is fixed at 6 dBm. (c) Simulation and (d) measurement results of mixing power P_{p-s} vs different signal power levels ($P_s = -4$ and $P_s = 6$ dBm), pump power P_p is fixed at 4 dBm.

Figs. 4(a) and 4(c). The nonlinear parameter of the AlN is extracted by fitting the circuit model to the experiment data and used for all the nonlinear simulations presented in this paper. The compliance modulation (ξ) for the resonator at $P_s = 6$ dBm is estimated to be 0.3%, which is comparable to AlN changes under large power in previous publications.^{23,34}

Finally, the parametric Q-enhancement phenomenon was simulated using the coupled multi-resonance circuit model and measured using the experimental setup detailed in the supplementary material. Figures 5(a) and 5(b) show the simulated and measured magnitude of admittance for the parallel resonance under different pump power levels. The pump frequency is fixed at the optimal frequency $f_p = 1364\,\mathrm{MHz}$. $P_p = -23\,\mathrm{dBm}$ is used as the reference case. Q-enhancement starts to be observed when pump power reaches 10 dBm and, then, increases with pump power. Pump power is raised until $P_p = 17\,\mathrm{dBm}$ because the device has poor power handling off the resonance frequency. The circuit model predicts similar trends as the experimental data, i.e., Q is enhanced with increasing pump power. The in-band hump in Fig. 5(b) is attributed to device specific IDT geometry fluctuations due to fabrication. This fabrication imperfection is not captured by the circuit model, which results in the admittance

shape difference between the simulation result and experiment data. Figures 5(c) and 5(d) show the simulated and measured magnitude of admittance for different pump frequencies. The pump power is fixed at the $P_D = 17$ dBm. Q-enhancement shows a dependency on the pump frequency because the proposed method relies on the idler resonance, which has a narrow bandwidth. The simulation predicts similar Q-enhancement dependency on pump frequency because the multiresonance behavior is captured by the circuit model. Q values under different pump power levels and frequencies are extracted from the admittance plot by 3 dB bandwidth method and plotted in Figs. 5(e) and 5(f). The linear increase in Q with pump power in Fig. 5(e) can be explained using the conclusion of the parametric mixing experiment. Material compliance modulation ξ increases linearly with pump amplitude; thus, the normalized negative conductance [from Eq. (3)] and quality factor increase linearly with pump power. Q in Fig. 5(f) is frequency dependent as the negative conductance depends on the idler resonance. Q is at a maximum when pump frequency is optimal at 1364, while Q is lowered when the pump frequency is away from 1364 MHz. These results verify the proposed parametric Q-enhancement method. Q is boosted 1.7 times (i.e., from 100 to 168) when the 17 dBm pump power is supplied. The 17 dBm pump power

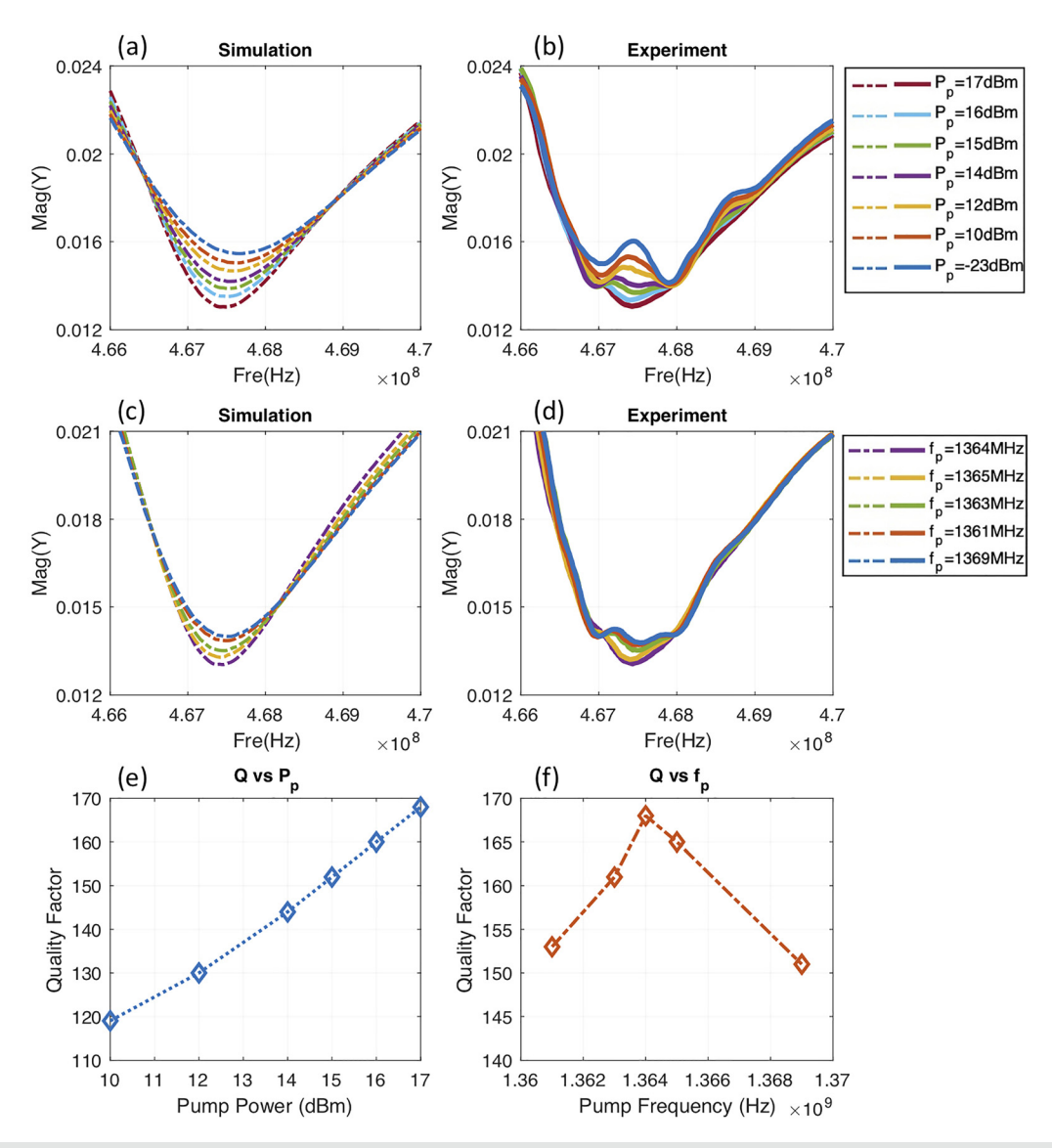


FIG. 5. Parametric Q-enhancement simulation and experiment results. (a) Simulated and (b) measured magnitude of admittance mag(Y) vs different pump power levels P_p . The pump frequency is fixed at $f_p = 1364$ MHz. (c) Simulated and (d) measured magnitude of admittance mag(Y) vs different pump frequencies f_p . The pump power is fixed at $P_p = 17$ dBm. Q vs (e) different pump power levels P_p and (f) different pump frequencies f_p .

is used in this work because the device has a very high insertion loss $(S21=-45\,\mathrm{dB})$ at the pump frequency f_p due to dispersion. The required pump power will be much lowered if the device is less dispersive through certain dispersion compensation and has a reduced insertion loss at the pump frequency f_p . It is also worth noting that if the method is applied to AlN Lamb wave resonators with higher quality factor (e.g., 1000), the normalized negative conductance seen by the signal path [from Eq. (3)] is increased, and thus, the quality factor will be further enhanced. This method can be readily applied to the high-Q AlN Lamb wave resonator with even greater Q-enhancement expected.

In this work, we explore a non-degenerate phase independent parametric Q-enhancement method for an AlN Lamb wave resonator. A multi-resonance coupled nonlinear model is developed to simulate the parametric coupling of each resonance and extract the nonlinearity of the AlN. Parametric effects and Q-enhancement have been demonstrated in both circuit simulation and experiment. The proposed Q-enhancement technique and multi-resonance coupled circuit model can be applied to other types of resonators that have nonlinear behavior and support multi-resonance operation.

See the supplementary material for a complete description of the negative-resistance parametric Q-enhancement concept, the coupled multi-resonance circuit model, and parametric mixing and Q-enhancement experiment setup.

This research was supported by the National Science Foundation EFRI NewLaw with the Award No. 1641128. The authors would also like to thank the staff of The Center of High Frequency Electronics, The Nanoelectronics Research Facility, and the Integrated System Nanofabrication Cleanroom for the use of their facilities.

DATA AVAILABILITY

The data that support the findings of this study are available from the corresponding author upon reasonable request.

REFERENCES

- ¹G. Piazza, "Contour-mode aluminum nitride piezoelectric MEMS resonators and filters," in in *MEMS-Based Circuits and Systems for Wireless Communication* (Springer, 2013), pp. 29–54.
- ²K.-Y. Hashimoto, Surface Acoustic Wave Devices in Telecommunications (Springer, 2000).
- ³K.-Y. Hashimoto, RF Bulk Acoustic Wave Filters for Communications (Artech House Publishers, 2009).
- ⁴G. Piazza, P. J. Stephanou, and A. P. Pisano, "Single-chip multiple-frequency ALN MEMS filters based on contour-mode piezoelectric resonators," J. Microelectromech. Syst. **16**(2), 319–328 (2007).
- ⁵G. Piazza, P. J. Stephanou, and A. P. Pisano, "Piezoelectric aluminum nitride vibrating contour-mode MEMS resonators," J. Microelectromech. Syst. 15(6), 1406–1418 (2006).
- ⁶M. Rinaldi, C. Zuniga, C. Zuo, and G. Piazza, "Super-high-frequency two-port AlN contour-mode resonators for RF applications," IEEE Trans Ultrason., Ferroelectr., Freq. Control 57(1), 38–45 (2010).
- ⁷C.-M. Lin, V. Yantchev, J. Zou, Y.-Y. Chen, and A. P. Pisano, "Micromachined one-port aluminum nitride Lamb wave resonators utilizing the lowest-order symmetric mode," J. Microelectromech. Syst. 23(1), 78–91 (2014).
- ⁸J. Zou, C.-M. Lin, A. Gao, and A. P. Pisano, "The multi-mode resonance in AlN Lamb wave resonators," J. Microelectromech. Syst. **27**(6), 973–984 (2018).
- ⁹C. Lam, G. Anming, C.-M. Lin, and J. Zou "A review of Lamé and Lamb mode crystal resonators for timing applications and prospects of Lamé and Lamb mode PiezoMEMS resonators for filtering applications," in Proceedings of the International Symposium Acoustic Devices Future Mobile Communication Systems (2018).
- 10 A. Gao and S. Gong, "Harnessing mode conversion for spurious mode suppression in AlN laterally vibrating resonators," J. Microelectromech. Syst. 25(3), 450–458 (2016).
- ¹¹J. Segovia-Fernandez, M. Cremonesi, C. Cassella, A. Frangi, and G. Piazza, "Anchor losses in AlN contour mode resonators," J. Microelectromech. Syst. 24(2), 265–275 (2015).
- ¹²A. Lozzi, L. G. Villanueva, and E. T.-T. Yen, "Anchor loss dependence on electrode materials in contour mode resonators," in *IEEE International Frequency Control Symposium (IFCS)* (IEEE, 2016), pp. 1–4.
- ¹³J. M. L. Miller, A. Ansari, D. B. Heinz, Y. Chen, I. B. Flader, D. D. Shin, L. G. Villanueva, and T. W. Kenny, "Effective quality factor tuning mechanisms in micromechanical resonators," Appl. Phys. Rev. 5(4), 041307 (2018).
- ¹⁴A. Gao, M. Winterkorn, Y. Yang, R. Lu, J. Provine, and S. Gong, "Boosting Qs of AlN resonators by redefining acoustic boundaries," in *IEEE 32nd International Conference on Micro Electro Mechanical Systems (MEMS)* (IEEE, 2019), pp. 883–886.

- ¹⁵C.-M. Lin, Y.-J. Lai, J.-C. Hsu, Y.-Y. Chen, D. G. Senesky, and A. P. Pisano, "High-Q aluminum nitride Lamb wave resonators with biconvex edges," Appl. Phys. Lett. 99(14), 143501 (2011).
- ¹⁶C. Xu, A. Kochhar, and G. Piazza, "Dynamic Q-enhancement in aluminum nitride contour-mode resonators," Appl. Phys. Lett. 115(17), 173504 (2019).
- 17 T. L. Naing, J. N. Nilchi, R. Liu, T. O. Rocheleau, and C. T. C. Nguyen, "Active Q-control for improved insertion loss micromechanical filters," in *IEEE International Frequency Control Symposium (FCS)* (IEEE, 2014), pp. 1–6.
- ¹⁸D. Rugar and P. Grutter, "Mechanical parametric amplification and thermomechanical noise squeezing," Phys. Rev. Lett. 67(6), 699–702 (1991).
- ¹⁹D. W. Carr, S. Evoy, L. Sekaric, H. G. Craighead, and J. M. Parpia, "Parametric amplification in a torsional microresonator," Appl. Phys. Lett. 77(10), 1545–1547 (2000).
- ²⁰C. Guo and G. K. Fedder, "A quadratic-shaped-finger comb parametric resonator," J. Micromech. Microeng. 23(9), 095007 (2013).
- ²¹J. Lee, C.-S. Li, Z. Wang, M.-H. Li, C.-H. Chin, S.-S. Li, and P. X. L. Feng, "Exploring parametric resonance effects in bulk-mode CMOS-MEMS resonators," in *IEEE International Frequency Control Symposium (FCS)* (IEEE, 2014), pp. 1–3.
- ²²I. Mahboob and H. Yamaguchi, "Piezoelectrically pumped parametric amplification and Q enhancement in an electromechanical oscillator," Appl. Phys. Lett. 92(17), 173109 (2008).
- ²³J. D. Schneider, T. Lu, S. Tiwari, X. Zou, A. Mal, R. N. Candler, Y. E. Wang, and G. P. Carman, "Frequency conversion through nonlinear mixing in acoustic waves," J. Appl. Phys. 128(6), 064105 (2020).
- ²⁴T. Lu, J. D. Schneider, X. Zou, S. Tiwari, Z. Yao, G. Carman, R. N. Candler, and Y. E. Wang, "Lamb wave resonator loaded non-reciprocal RF devices," in *IEEE/MTT-S International Microwave Symposium (IMS)* (IEEE, 2020), pp. 516–519.
- ²⁵R. Engelbrecht, "Parametric energy conversion by nonlinear admittances," Proc. IRE 50(3), 312–321 (1962).
- ²⁶P. K. Tien, "Parametric amplification and frequency mixing in propagating circuits," J. Appl. Phys. 29(9), 1347–1357 (1958).
- ²⁷L. K. Yeung, X. Zou, and Y. E. Wang, "Parametric quality factor enhancement for highly-selective miniaturized BPFs," in *IEEE Radio and Wireless Symposium (RWS)* (IEEE, 2020), pp. 148–151.
- ²⁸L. K. Yeung, X. Zou, and Y. Wang, "Parametrically enhanced bandpass filters," IET Microwaves, Antennas Propag. 15, 229 (2021).
- ²⁹D. M. Pozar, *Microwave Engineering* (John Wiley & Sons, 2011).
- 30T. Lu, J. D. Schneider, Z. Yao, G. Carman, and Y. E. Wang, "Nonlinear surface acoustic wave grating for parametric amplification," in *IEEE Radio and Wireless Symposium (RWS)* (IEEE, 2019), pp. 1–3.
- ³¹Y. Wang, W. L. Goh, K. T. Chai, X. Mu, Y. Hong, P. Kropelnicki, and M. Je, "Parasitic analysis and π-type Butterworth-Van Dyke model for complementary-metal-oxide-semiconductor Lamb wave resonator with accurate two-port Y-parameter characterizations," Rev. Sci. Instrum. 87(4), 045004 (2016)
- 32S. Tiwari, Dynamics of Multiferroic Coupling (UCLA, 2020).
- 33R. H. Olsson, K. E. Wojciechowski, and D. W. Branch, "Origins and mitigation of spurious modes in aluminum nitride microresonators," in *IEEE International Ultrasonics Symposium* (IEEE, 2010).
- 34E. Defay, N. Ben Hassine, P. Emery, G. Parat, J. Abergel, and A. Devos, "Tunability of aluminum nitride acoustic resonators: A phenomenological approach," IEEE Trans Ultrason., Ferroelectr., Freq. Control 58(12), 2516–2520 (2011).